Analysis of Initial Reactions of MALDI Based on Chemical Properties of Matrixes and Excitation Condition

Yin-Hung Lai,[†] Chia-Chen Wang,[‡,†] Chiu Wen Chen,[†] Bo-Hong Liu,[†] Sheng Hsien Lin,[§] Yuan Tseh Lee,[†] and Yi-Sheng Wang*,[†,‡]

[†]Genomics Research Center, Academia Sinica, Taipei 115, Taiwan

[‡]Institute of Biochemistry and Molecular Biology, National Yang-Ming University, Taipei 112, Taiwan

[§]Department of Applied Chemistry, National Chiao Tung University, Hsinchu 300, Taiwan

S Supporting Information

ABSTRACT: This investigation concerns the initial chemical reactions that affect the ionization of matrixes in matrix-assisted laser desorption/ionization (MALDI). The study focuses on the relaxations of photon energy that occur on a comparable time scale to that of ionization, in which the available laser energy is shared and the ionization condition is changed. The relaxations include fluorescence, fragmentation, and nonradiative relaxation from the excited state to the ground state. With high absorption cross section and long excited-state lifetime, photoionization of matrix plays an important role if sufficient laser energy is used. Under other conditions, thermal ionization of the molecule in the ground state is predicted to be one of the important reactions. Evidence of change in the branching ratio of initial reactions with the matrix and the excitation wavelength was obtained with α-cyano-4-hydroxycinnamic acid, sinapinic acid, 2,5-dihydroxybenzoic acid, and 2,4,6-trihydroxyacetophenone. These matrixes are studied by obtaining their mixed crystal absorption spectra, fluorescence properties, laser-induced infrared emission, and product ions. The exact ionization pathway depends on the chemical properties of matrixes and the excitation conditions. This concept may explain the diversity of experimental results observed in MALDI experiments, which provides an insight into the ensemble of chemical reactions that govern the generation of ions.
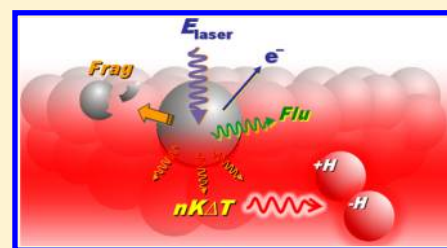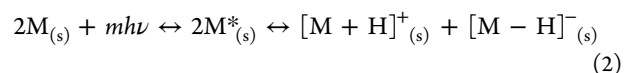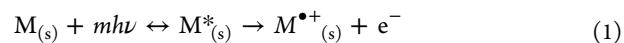
INTRODUCTION

Matrix-assisted laser desorption/ionization (MALDI) is one of the most important ionization techniques in biological mass spectrometry.[1−4] It has been successfully utilized in proteomic studies because of its high speed and sensitivity,[5,6] but its complicated optimization process limits its application in many research fields.[7−9] The lack of detailed knowledge of the ionization also disfavors quantitative analysis. To optimize the performance of MALDI-based mass spectrometry for biological studies, a detailed understanding of the mechanism of MALDI is urgently needed.

In the last two decades, several reaction models have been proposed to explain MALDI.[10−23] The most important concept involves the ionization of matrix molecules, followed by charge transfer from the matrix ions to the analytes.[9] Among other reaction details, a major debate continues over whether the matrix ions are produced via multiphoton excitation,[16,24−26] annihilation/energy pooling processes,[20,24,27] an excited-state thermoionic emission process,[10,28] or whether they are precharged in the crystal.[11,15] However, attempts to establish an exclusive reaction model that converges with existing knowledge have encountered great difficulties, such as describing the dramatic variation of experimental results with the change of the matrix,[24,29] the matrix-to-analyte ratio,[30,31] the morphology of the sample,[32,33] and the excitation method.[34] Except for the precharging concept, the most likely

pathways of primary ionization can be qualitatively divided into election depletion and proton-pair production, if categorized on the basis of the identity of product ions.[10] The simplified reaction formulas of the two pathways are

$$M_{(s)} + mh\nu \leftrightarrow M^*_{(s)} \rightarrow M^{\bullet+}_{(s)} + e^- \tag{1}$$

$$2M_{(s)} + mh\nu \leftrightarrow 2M^*_{(s)} \leftrightarrow [M + H]^+_{(s)} + [M - H]^-_{(s)} \tag{2}$$

in which M and M* denote the matrix molecules in their ground and excited states, respectively. Equation 1 is photoionization, which may involve a sequential multiphoton absorption or annihilation mechanism.[10,20,24,27,35] The evidence for eq 1 is the presence of radical ions in many matrixes with low laser fluence (F).[24,26,36] Equation 2 is also an important candidate for the primary reaction because protonated and deprotonated molecules are the major products under typical MALDI conditions. It has also been predicted to be energetically more favorable than photoionization,[10] but proton-disproportionation in the excited state has been considered to be unfavorable for commonly used matrixes.[19]

Thus, it is worth further studying whether eq 2 can occur under other conditions, such as in the ground state.

Analyses of photoelectrons and ion pairs are important to the study of the matrix ionization.[10,37−41] Frankevich et al.[42] and Knochenmuss[38] reported that the origin of photoelectrons is closely associated with the substrate. Dashtiev et al.[39] and Knochenmuss[40] recently also discussed the correlation between positive and negative ion yields. While the commercial instruments used by these authors allowed only an indirect study of these issues, a method for direct analysis is still necessary. We recently re-examined these topics using synchronized dual-polarity time-of-flight mass spectrometry.[43−45] In such series of studies, strong evidence of eq 1 for 2,5-dihydroxybenzoic acid (DHB) was obtained. Interestingly, the threshold laser fluence (F_{th}) for producing photoelectrons was lower than that for matrix ions. In our studies, the difference in F_{th} between photoelectron and ion generation increased dramatically in the order 2,4,6-trihydroxyacetophenone (THAP) < sinapinic acid (SA) < DHB. If the different F_{th} values for ions and photoelectrons resulted from different ionization channels, the details of the ionization reactions in DHB and THAP should differ markedly. These observations disfavor the use of a single model to explain every case of MALDI because the respective matrixes were ionized under unique reaction environments.

Many chemical reactions consume energy and may affect ion production. The system temperature increase, for example, is an essential factor in MALDI, but the data obtained from different methods disagree with each other, including the results of the infrared emission,[46] the survival yields of thermometer molecules,[47−50] the internal energy of molecules,[50,51] and the theoretical simulations.[52,53] The impact of fluorescence on ionization is also a matter of debate, and the first excited-state lifetimes (τ_1) in the literature vary considerably; for example, the τ_1 values of DHB reported by Ludemann et al. and Allwood et al. are 0.6 and 7.7 ns, respectively.[35,54,55] The variation of τ_1 is probably due to the fact that τ_1 is short in comparison with the duration of nanosecond lasers, so it was enveloped within the excitation pulse. Measurements of fluorescence lifetime also differ, perhaps because of the use of different laser fluence or different contributions from the solid phase and the expanding plume.[20,54,55] Therefore, important chemical reactions in MALDI must still be systematically analyzed.

This study discusses the relationship between ionization and other initial chemical reactions of MALDI. The absorbed laser energy is assumed to be dissipated rapidly via multiple pathways and subsequently change the ionization condition. These pathways include radiative relaxations of fluorescent matrixes and nonradiative relaxations of all matrixes. The important results concerning nonradiative relaxation include not only an increase of system temperature but also the decomposition and the ionization of matrixes. Accordingly, eqs 1 and 2 and other endoergic reactions occur in parallel, and their branching ratio depends on the chemical characteristics of the matrix and the excitation conditions. A dynamic balance of the contribution of the reactions should be satisfied in every experiment. The mixed crystal absorption spectra of four model matrixes, including α-cyano-4-hydroxycinnamic acid (CHCA), DHB, SA, and THAP, were obtained quantitatively. The absorption cross section (σ) of the matrixes, the fluorescence properties, the IR emission intensities, and the fragment abundances were used to elucidate the redistribution of energy.

Taking into account multiple ionization pathways, the concept of energy competition is used to resolve the ambiguity of reaction models that explain MALDI using a single ionization scheme. The quantitative prediction of the appearance of ion signal is not included in the present study because the final ion signal also depends on the chemical equilibrium between ions and neutral molecules, as well as the desorption process.[13]

■ EXPERIMENTAL SECTION

The UV absorption spectra were recorded by a commercial absorption spectrometer (U-3310, Hitachi High-Technologies Co., Tokyo, Japan). A built-in integrating sphere with a diameter of 60 mm was used to minimize the scattering loss in this study. Sample pellets of 13 mm in diameter and 1.5−2.0 mm in thickness were prepared using approximately 500 mg of sample powders by a hydraulic press. To disperse and reduce the size distribution of the powders before pressing, they were stirred manually by a micro spatula for 30 min. The powders were mixed thoroughly with barium sulfate in molar ratios of 1/600 to 1/25600. The ratio ranges were selected to avoid saturation of the signal in the respective cases. Baseline calibration was performed with a pure barium sulfate pellet. The value of σ was derived from the slope of the matrix concentration versus absorbance (see the Supporting Information), and its uncertainty was determined by the error propagation of the data.

Fluorescence lifetime imaging microscopy (FLIM) was recorded using a confocal microscope (Leica TCS SP5, Leica Microsystems CMS GmbH, Mannheim, Germany). The solid matrixes, prepared by the dried droplet method, were irradiated by an 80 MHz pulse laser with a wavelength (λ_{laser}) of 710 nm and a pulse duration of 140 fs (Chameleon Ultra II, Coherent, Santa Clara, CA, USA). The time-resolved laser-induced fluorescence was detected from 420 to 500 nm and 500 to 550 nm for DHB and CHCA, respectively. The fluorescence was analyzed in the one-color, two-photon excitation process, using a single-photon counting system (PicoHarp 300 and SymPhoTime, PicoQuant GmbH, Berlin, Germany) that provides a time resolution of 4 ps. Intensity decays within 1 and 12.4 ns after the maximum fluorescence signal were fitted to a double exponential function in order to describe the data accurately. The method provided τ_1 with an accuracy of better than 95%. When calibrated using a 4′,6-diamidino-2-phenylindole with a double strand DNA, an average τ_1 obtained herein was 2.28 ± 0.03 ns, which agreed perfectly with the value in a previous report (2.20 ns).[56]

To record the fluorescence spectra, pure matrix pellets were analyzed by a spectrofluorometer (FluoroMax-3, Horiba Advanced Techno Co., Ltd., Kyoto, Japan). The reflected and stray light was reduced by a filter that was installed in front of the monochromator, and by aligning the incident beam to about 30° from the illuminated surface. On the basis of the assumption that the detection efficiency is independent of wavelength, the fluorescence spectra of the solid-phase matrixes were obtained.

Infrared emission was measured using two types of fast InGaAs PIN photodiodes which covered the spectral ranges from 0.9 to 1.7 μm (G8376-03, Hamamatsu Photonics K.K., Shizuoka, Japan) and 1.2 to 2.6 μm (FGA20, Thorlabs Inc., New Jersey, USA). The photodiodes were driven by an OP amplifier (OPA847/DEM-OPA-SO-1B, Texas Instruments Inc., Texas, USA). An IR grade fused-silica double lens system (F/# = 1, Dia. = 50.8 mm) was used to focus the IR photons

onto the photodiodes. Stray light was attenuated with a long-pass optical filter (RG-830, Edmund Optics Inc., New Jersey, USA) that was installed in front of the photodiodes. The MALDI samples were prepared by the dried droplet method and enclosed in a vacuum chamber with a pressure of 5×10^{-7} mbar. The samples were irradiated with photons of three laser wavelengths (λ_{laser}), including 337 nm, output from a nitrogen laser (VSL-337ND-S, Spectra-Physics Inc., California, USA), and 266 and 355 nm, output from an Nd:YAG laser (MINILITE I, Continuum Electro-Optics Inc., California, USA). The pulse duration of the lasers was approximately 3–5 ns. The laser beam was focused to a spot with a diameter of roughly 100 μm, and it examined the sample at an angle of 40° from the surface normal. Surface temperatures were derived from the IR emission signal assuming that blackbody radiation is satisfied, as reported by Koubenakis et al.[46] The data was typically averaged over 200 laser shots.

All mass spectra were obtained using a mass spectrometer that was made in the laboratory, as described elsewhere.[57] Briefly, the mass spectrometer consisted of a MALDI ion source and a 2.1 m linear flight tube. The same laser and focusing condition for the detection of IR emission was utilized to produce the ions. The ions were accelerated by a DC high voltage of ±20 kV and without delayed extraction. The mass spectra were averaged over typically 100 shots. The mass assignments were further examined with a Fourier-transform ion cyclotron resonance mass spectrometer (Apex Ultra 94, Bruker Daltonics Inc., Billerica, MA, USA).

The gas-phase reaction Gibbs free energy was estimated from the most stable structures using the Gaussian 03 package. The calculation was also operated with the polarizable continuum model based on self-consistent reaction field theory.[58,59] The molecular geometry optimization and vibrational frequency calculations were made using density functional theory with the B3LYP/6-31+g (d, p) basis set.

All chemicals were obtained from Sigma Aldrich (Sigma-Aldrich Co., Missouri, USA) and were used without further purification. The matrixes were dissolved in acetonitrile/water (50/50) to a concentration of 0.1 M before deposition. For measuring the mass spectra and the IR emission, 2 and 10 μL of sample solution were vacuum-dried on the sample surface, respectively.

RESULTS AND DISCUSSION

Rapid Energy-Dissipation Pathways. In MALDI, prompt endoergic reactions compete with matrix ionization for the absorbed laser energy. Since the duration of lasers is typically 3–5 ns, only reactions that occur on a comparable time scale are significant. The reactions start from the absorption of laser photons by the matrix crystals. The absorption of near UV photons results in the electronic transition of the matrix from the ground state (S0) to the first excited state (S1):

$$M_{S0(s)} + mh\nu \rightarrow M_{S1}{}^*{}_{(s)} \tag{3}$$

where $M_{S1}{}^*$ is a possible analogue of M^* in eqs 1 and 2. Apart from photoionization following absorption or annihilation of the second photon energy, $M_{S1}{}^*$ can undergo fragmentation, relaxation via vibrational relaxation (VR), internal conversion (IC), or fluorescence. Ionization may also occur at high temperature conditions when the photon energy is converted to the thermal energy of $M_{S0}{}^*$, as will be discussed later. The typical reaction pathways are illustrated in Figure 1.
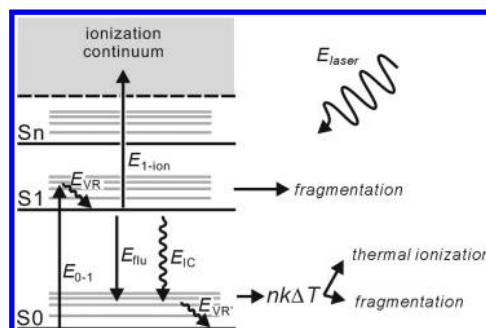
Figure 1. The representative reaction pathways of a solid matrix molecule when it is excited by UV laser photon.

The overall reaction can be interpreted as the redistribution of the absorbed laser energy (E_{laser}) into four primary components, including energy for photoionization (E_{pi}), fragmentation of $M_{S0}{}^*$ and/or $M_{S1}{}^*$ (E_{frag}), as well as fluorescence (E_{flu}) and nonradiative relaxation (E_{nonrad}) from $M_{S1}{}^*$ to $M_{S0}{}^*$. Thus, the energy balance equation is

$$E_{laser} = aE_{pi} + bE_{frag} + cE_{flu} + dE_{nonrad} \tag{4}$$

where a, b, c, and d are the branching ratios of molecules that are associated with the respective energy dissipation channels. In Figure 1, E_{VR} is the relaxation energy in the excited state. The nonradiative relaxations include the IC from $M_{S1}{}^*$ to $M_{S0}{}^*$ and the subsequent VR processes ($E_{VR'}$). Therefore, the expressions for E_{pi} and E_{nonrad} become

$$E_{pi} = E_{0-1} - E_{VR} + E_{1-ion} \tag{5a}$$

$$E_{nonrad} = E_{VR} + E_{IC} + E_{VR'} \tag{5b}$$

The IC and VR processes convert the energy into thermal energy. The dE_{nonrad} is eventually converted into $nK\Delta T$, where ΔT is of the order of several hundreds of Kelvin with typical MALDI conditions.[26,28,46,47,49,50] Such a high-temperature environment may initiate thermal reactions, including decomposition, ionization, and other chemical reactions. Therefore, the energy consumed in the thermal ionization of $M_{S0}{}^*$ is included in E_{nonrad}. In the current study, the consumed energy for thermal decomposition is combined with the excited-state fragmentation because the experimental data herein cannot distinguish one from another. The residual temperature after these prompt reactions contributes to the desorption of the matrix. Notably, the energy that is required for the disintegration of precharged species in the lucky survivor model[11,15] can also be included in E_{nonrad} because photoionization is considered unimportant in the precharging process.

Since the configurations of energy levels of matrixes are unknown, the branching ratio of every component in eq 4 varies. Therefore, the matrix ion yield cannot be determined with reference to a single ionization mechanism. Even for the same matrix, the branching ratios may change with the excitation conditions. The components indicated in eq 4 for different matrixes are discussed below.

Mixed Crystal Absorption Spectra (E_{laser}). The energy available in MALDI is determined by the σ of the matrix at the λ_{laser}. The absorption spectra of CHCA, SA, and DHB all include a similar primary absorption above 300 nm and a shoulder of a secondary absorption that peaks below 250 nm, as displayed in Figure 2. THAP yielded only one distinctive

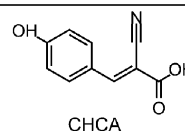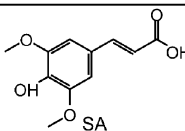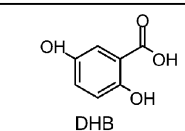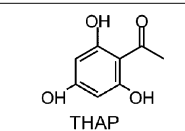absorption at 286 nm. In no case was absorption observed above 650 nm.
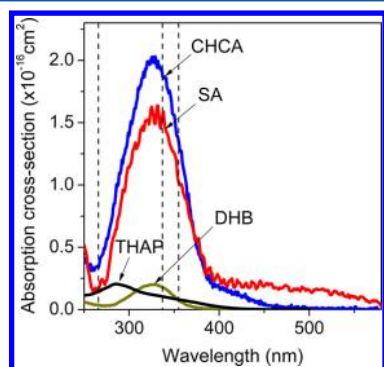
Figure 2. Calibrated mixed crystal UV absorption spectra of the studied matrixes.

The absolute σ values were estimated on the basis of the observations in this study and the result of Allwood et al.[60] In Figure 2, the intensity of the spectrum of DHB was scaled linearly to the reference data, according to the σ value at 337 nm (σ_{337}). DHB was selected for the calibration because the thickness of the sample that was prepared by sublimation in the work of Allwood et al. had been carefully measured. The spectra of other matrixes obtained herein were subsequently calibrated according to the relative σ_{337}. In comparison with the sublimation method, the advantage of the mixed crystal method is that the matrix concentration in the solid state can be precisely determined, so the reported σ values provide an important basis for the subsequent analysis. The changes of absorbance of the matrixes with the concentration are shown in the Supporting Information, and the structure of the matrixes and their σ_{266}, σ_{337}, and σ_{355} are summarized in Table 1.

Because the laser penetration depth is inversely related to σ, the resultant energy densities in the matrix crystals depend on λ_{laser} if a fixed F is used. Our data indicate that σ_{337} and σ_{355} of the matrixes decreased in the order CHCA > SA > DHB > THAP, whereas σ_{266} decreased in the order CHCA > SA > THAP > DHB. In one extreme case, the resultant energy density of THAP is approximately 7% that of SA when excited by the 337 nm laser, because σ_{337} of THAP is about 15 times lower. However, the same energy density can be obtained for THAP and SA if a 266 nm laser is used. Clearly, the E_{laser} per unit volume in eq 4 depends on the matrix property and λ_{laser}, so the mechanistic studies of ionization should consider both factors.

Photoionization (E_{pi}). Photoionization is important for matrixes with high σ and long τ_1. This process may include both sequential multiphoton excitation and annihilation. It should be emphasized that, although the annihilation model resolved the difficulty when explaining the photoionization with three-photon absorption processes and adequately described some obervations,[20,27,35] the theoretical prediction and the observation of photoelectrons suggested that two 337 nm laser photons are sufficient to ionize solid DHB.[45] In fact, it is well-known that the ionization potential of aromatic derivatives normally lies below twice the energy of the S1 state, as discussed extensively in zero kinetic energy photoelectron and resonance enhanced multiphoton ionization spectroscopies.[61] Therefore, if the first photon manages to promote the matrix to the S1 state, the second photon is likely sufficient to ionize the

Table 1. Structure of the Studied Matrixes and Their Absorption Cross Section at Commonly Used Laser Wavelengths

	Absorption Cross-Section (cm^2)		
	266 nm	337 nm	355 nm
CHCA	3.40×10^{-17} $\pm 8.50 \times 10^{-18}$	1.89×10^{-16} $\pm 4.53 \times 10^{-17}$	1.35×10^{-16} $\pm 3.78 \times 10^{-17}$
SA	1.51×10^{-17} $\pm 4.39 \times 10^{-18}$	1.56×10^{-16} $\pm 4.37 \times 10^{-17}$	1.03×10^{-16} $\pm 2.67 \times 10^{-17}$
DHB	3.58×10^{-18} $\pm 2.43 \times 10^{-19}$	1.84×10^{-17} $\pm 1.10 \times 10^{-18}$	8.15×10^{-18} $\pm 3.42 \times 10^{-19}$
THAP	1.44×10^{-17} $\pm 2.05 \times 10^{-18}$	1.05×10^{-17} $\pm 2.31 \times 10^{-18}$	7.95×10^{-18} $\pm 1.56 \times 10^{-18}$

matrix. Under such conditions, the σ of M_{S1} can be much higher than that of M_{S0}, or the absorption of the second photon can be saturated if it promotes the molecule to ionization continuum.[62] Thus, the sequential multiphoton excitation can adequately describe the fluorescence of DHB as a function of F (see the Supporting Information), and it should be reconsidered as an important reaction pathway that depopulates M_{S1}.

One of the most important signatures of photoionization is the presence of radical ions near F_{th}. The Supporting Information includes the mass spectra that were recorded with 266 and 355 nm lasers near the respective F_{th}. The important features and the normalized intensities were summarized in Table 2. The radical cations in CHCA, SA, and DHB were the most abundant features that were obtained using the 266 nm laser. The use of the 355 nm laser markedly reduced the abundance of the radical cations, suggesting that the abundance of photoionization decreased when switching λ_{laser} from the middle UV (i.e., 266 nm) to the near UV (i.e., 337 and 355 nm) range.

Notably, it is difficult to apply the annihilation model to the ionization of THAP and SA, since their τ_1 should be on the order of a low picosecond range or shorter.[63] Such a value is shorter than the proposed annihilation rate, i.e., on the order of subnanosecond or longer. The most important evidence was the absence of THAP radical ions when the 355 nm laser was used, although its radial cation became the most intense feature when the 266 nm laser was used. The absence of THAP radical ions with near UV laser is attributed to its short τ_1 and the low σ. An interesting result is the presence of SA radical cations when the 355 nm laser is used, even though its τ_1 is short. It can be attributed to the high σ in that region, so the absorption of the second photon may be very efficient. Further study is necessary to elucidate the relative contribution of annihilation and multiphoton absorption to the ionization in every case.

Table 2. Relative Abundance of Mass Spectral Features of the Examined Matrixes Excited by 266 and 355 nm Lasers near the Respective F_{th}

matrix	266 nm	355 nm
CHCA	$[m]^{\bullet+}$ 1; $[m-H]^{-}$ 1; $[m-COOH]^{+}$ 0.88; $[m]^{\bullet-}$ 0.3; $[m+H]^{+}$ 0.78; $[m-COOH]^{-}$ 0.15; $[m+2H]^{+}$ 0.28; $[m+H-H_2O]^{+}$ 0.28; others 0.16	$[m]^{\bullet+}$ 1; $[m-H]^{-}$ 1; $[m+H-H_2O]^{+}$ 0.85; $[m]^{\bullet-}$ 0.33; $[m+2H]^{+}$ 0.23; $[m-COOH]^{-}$ 0.07; $[m]^{\bullet+}$ 0.18
SA	$[m]^{\bullet+}$ 1; $[m-H]^{-}$ 1; $[m+H]^{+}$ 0.73; $[m-H-CH_3]^{-}$ 0.18; $[m+H-H_2O]^{+}$ 0.66; $[m-H-C_2H_6]^{-}$ 0.11; $[m+2H]^{+}$ 0.19; $[m]^{\bullet-}$ 0.1	$[m+H-H_2O]^{+}$ 0.59; $[m-H]^{-}$ 0.22; $[m+H]^{+}$ 0.26; $[m-H-CH_3]^{-}$ 0.1
DHB	$[m]^{\bullet+}$ 1; $[m-H]^{-}$ 1; $[m+H-H_2O]^{+}$ 0.51; $[m]^{\bullet-}$ 0.49; $[m+H]^{+}$ 0.16; $[m-2H]^{-}$ 0.19	$[m]^{\bullet+}$ 1; $[m-H]^{-}$ 1; $[m+H-H_2O]^{+}$ 0.74; $[m-2H]^{-}$ 0.5; $[m+H]^{+}$ 0.69; $[m]^{\bullet-}$ 0.4
THAP	$[m]^{\bullet+}$ 1; $[m-H]^{-}$ 1; $[m+H]^{+}$ 0.91; $[m]^{\bullet-}$ 0.47; $[m-CH_3]^{+}$ 0.22	$[m+H]^{+}$ 1; $[m-H]^{-}$ 1; $[m+2H]^{+}$ 0.18

Excited-State and Ground-State Fragmentations (E_{frag}).

The fragmentations consume photon energy by breaking chemical bonds. Commonly observed fragmentation products of matrixes include dehydration and decarboxylation.[36,64−66] In the present work, the most important fragments were the dehydration products ($[M+H−H_2O]^{+}$) in CHCA, DHB, and SA, when the respective F_{th} of the 355 nm laser was used. With the same laser condition, demethylation ($[M−H−CH_3]^{-}$) and decarboxylation ($[M−COOH]^{-}$) were detected only in the spectra of SA and CHCA, respectively. The only matrix without fragmentation when excited by the 355 nm laser was THAP (Table 2).

When λ_{laser} was changed from 355 to 266 nm, new fragments were detected from all matrixes except the same fragment was observed in DHB. The new representative features included $[M−COOH]^{+}$ in CHCA and SA, $[M−H−C_2H_6]^{-}$ in SA, and $[M−CH_3]^{+}$ in THAP. A similar result has been reported previously for SA.[67,68] These new fragments could only be detected with high F when the 355 nm laser was used, indicating that the 266 nm laser induced harsher environments than did the 355 nm laser. This result implies that changing laser conditions may activate different thermal decomposition channels. Hence, the efficiencies and the details of the mechanism of thermal dissipation depend on λ_{laser} and F.

Although the spectral pattern reveals information on the extent of fragmentation, the detailed fragmentation mechanism is unavailable. For instance, fragmentation may occur in M_{S1}^{*} via repulsive states or after internal conversion from M_{S1}^{*} to M_{S0}^{*}, but it is difficult to determine their relative abundance. A recent study that involved the photoexcitation of gaseous DHB concluded that the elimination of H from the meta-OH group is a reaction that proceeds via a repulsive excited state, whereas the elimination of H_2O occurs in the ground state.[69] The excited-state fragmentation seems to play a minor role in DHB, but further experiments are necessary to verify its contribution in the solid state and in other matrix molecules.

Fluorescence Relaxation (E_{flu}).

When excited by the near and middle UV lasers, only CHCA and DHB fluoresced within the range 365−700 nm. Thus, the value of c in eq 4 is negligible for SA and THAP. The τ_1 values of DHB and CHCA that were estimated from the FLIM measurements were 0.64 ± 0.14 and 1.39 ± 0.24 ns, respectively, as shown in Figure 3. The value of DHB agreed with that reported by Ludemann et al.,[35] suggesting that the fluorescence competes with ionization on the same time scale for available energy.

The fluorescence spectrum of DHB includes a broad feature peaking at approximately 417 nm with a width of roughly 90 nm, as presented in Figure 4. This result was similar to the data of Allwood et al.[54] and Ehring et al.[70] In contrast, the spectrum of CHCA includes a major peak at approximately 519 nm with a width of about 130 nm. This spectral shape differs from that reported by Allwood and Dyer, in that the data herein has a higher intensity at longer λ side. This difference is probably due to the different crystalline structures and the different F values that were used to obtain the data.

Notably, the same spectral features were obtained in all three excitation wavelengths used in this study, indicating that the fluorescence was emitted from the same electronic state. This result suggests that the relaxation of DHB and CHCA still goes through the S1 state when the 266 nm laser is used. Although a middle UV laser may excite the matrixes to a higher excited state (Sn), the IC to the higher vibrational levels of the S1 state may be too fast to allow direct fluorescence from that higher
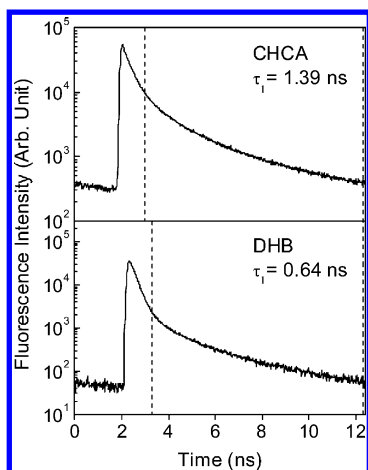
Figure 3. Time-resolved fluorescence of solid-phase CHCA and DHB. The vertical lines denote the data ranges used to estimate the first excited-state lifetimes.
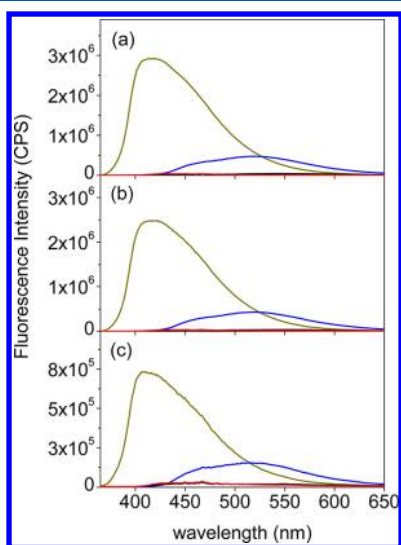
Figure 4. Fluorescence spectra of solid-phase matrixes excited by 355 nm (a), 337 nm (b), and 266 nm (c), respectively. Blue curve represents CHCA; red curve represents SA; dark yellow curve represents DHB; black curve represents THAP.

excited state (S_n). Therefore, the probability of photoionization with middle UV lasers may be increased because the molecule is expected to spend a longer time in the S1 state, as well as the higher σ of the M_{S1}^*, since the middle UV can excite the matrix to the ionization continuum with a higher density of state than that by near UV. This may also explain the presence of radical cations of SA and THAP when the 266 nm laser was utilized.

The integrated fluorescence intensities (I_{flu}) of CHCA and DHB obtained herein and by Allwood et al. suggest that the radiative relaxation in DHB is more important than CHCA. The I_{flu} of CHCA was roughly 25% that of DHB, but its σ_{337} was an order of magnitude higher. Because the τ_1 of CHCA is also double that of DHB, CHCA may undergo eq 1 with a comparable F_{th} to that of DHB. A preliminary study of the appearance of photoelectrons supported this prediction (data not shown).

Nonradiative Relaxation (E_{nonrad}). Nonradiative relaxation converts photon energy to the thermal energy of the matrixes in their ground state. It plays an important role because the IC

and VR processes occur within the nanosecond range, which is orders of magnitude faster than thermal conduction in the solid matrix.[46] Such thermal energy causes an abrupt heating of the system and induces multiple reactions. A similar high-temperature environment may also be produced by laser photons of long λ_{laser} that is insufficient to induce electronic transition, such as in IR-MALDI.[34,71−73] On the other hand, the desorption and concurrent thermal reactions, including thermal fragmentation and ionization, may efficiently retard the temperature rise.[13]

(a) System Temperature Increase. Changes of matrix temperature can be evaluated by measuring the infrared emission, if the assumption is made that the emission coefficients of the matrixes are similar.[46] In the present study, the typical MALDI condition was reproduced by well-focused laser beams that were used to excite matrixes in a vacuum. As listed in Table 3, the observed IR emission intensities (I_{IR}) in

Table 3. The IR Signal Intensity (mV) of the Studied Matrixes with Laser Fluence = 100 J/m²

detecting range	infrared 1 (0.9−1.7 µm)			infrared 2 (1.2−2.6 µm)		
excitation wavelength (nm)	266 nm	337 nm	355 nm	266 nm	337 nm	355 nm
CHCA	8.5	7.5	5.7	8.3	6.4	4.4
SA	1.8	4.5	5.6	2.5	5.5	2.3
DHB	1.5	3.9	2.5	2.3	3.7	2.1
THAP	24.7	52.6	50.9	20.9	25.5	29.2

the two detected IR ranges decreased in the order THAP > CHCA > SA ≥ DHB. This result was obtained consistently at the three λ_{laser} values when the typical fluence range of MALDI was used. Using the data of the type I photodiode obtained with the 337 nm laser in Table 3, the estimated temperatures of THAP, CHCA, SA, and DHB are 785.3, 691.4, 668.7, and 662.5 K, respectively. The order of THAP and DHB agrees with the result for thin matrix layers that was obtained by Koubenakis et al.[46] but disagrees with the result of thick matrix layers in the same literature and that by Schulz et al.[47] It needs to be emphasized that the data of all temperature estimation methods should be considered with care. The accuracy in temperature calibration with existing knowledge and technology for quantitative analyses is still questionable.

A surprising result was that the I_{IR} value of THAP was highest of all, although its σ_{337} and σ_{355} values were the lowest. For example, its I_{IR} was, on average, 10 times that of DHB when it was excited by the 337 nm laser, but its σ_{337} was roughly 40% lower. In contrast, the order of the I_{IR} of CHCA, SA, and DHB at every λ_{laser} agreed reasonably with the corresponding value of σ. The unique IR emission property of THAP can also be seen under various excitation conditions. Figure 5 plots the change in I_{IR} with the effective F of the three λ_{laser} values. The effective F were the observed F, corrected according to the σ of the respective matrixes. For CHCA, SA, and DHB, the slopes of the data obtained with the 337 and 355 nm lasers were similar, and they were about half that obtained with the 266 nm laser. For the THAP, in contrast, the slope with the 337 and 355 nm lasers was roughly 2−3 times that with the 266 nm laser. A rational explanation is that most of the energy dissipation pathways were inactive in THAP when the 337 and 355 nm laser were used, so the relaxation of photon energy favored the accumulation of thermal energy. When the
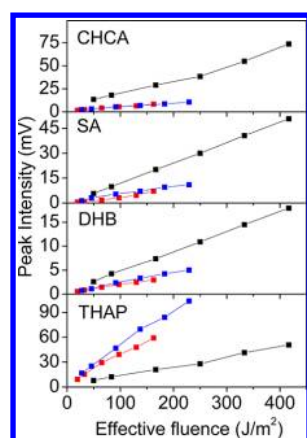
Figure 5. IR emission of the solid-phase matrixes obtained with various effective fluences of the three laser wavelengths. Black squares were obtained with the 266 nm laser; red squares were obtained with the 337 nm laser; blue squares were obtained with the 355 nm laser.

266 nm laser was used, however, the fragmentation and photoionization of THAP were activated and they retarded the increase of the system temperature.

(b) Thermal Ionization. Quantum chemistry calculation suggests that eq 2 is thermodynamically favorable. The energy barrier could be overcome in the high-temperature environment of MALDI. Although the production of $[M+H]^+$ and $[M-H]^-$ may also be attributed to the secondary reactions subsequent to photoionization, it is difficult to rationalize that the radical ion was absent from the mass spectrum of THAP when it was excited by the 355 nm laser. In fact, $[M+H]^+$ and $[M-H]^-$ were the only ions detected in THAP when the 355 nm laser was operated at the F_{th} value of THAP.

According to the *ab initio* calculation, eq 2 has a reaction enthalpy (ΔH) of 4.92 eV for gaseous $THAP_2$. It is significantly lower than the predicted ionization potential of $THAP_2$ (6.96 eV). The predicted ΔH value of eq 2 is further reduced dramatically to 3.54 eV when a dielectric constant of 2.38 is utilized in the calculation. This dielectric constant was used because the matrixes were tightly embedded in the crystal, and the value for toluene was selected, since the value of THAP was unavailable. The impact of the dielectric constant on ΔH is likely to be underestimated because the dielectric constant of acetophenone is 17.44.[74] The new effective ΔH can be easily overcome by a single laser photon, and the thermal ionization may become a major pathway. The electron-disproportionation of ground-state $THAP_2$ has a predicted ΔH value of 7.52 eV, which is much higher than that of proton-disproportionation and should not make a significant contribution in this case. Therefore, the result suggests that eq 2 may be a favorable pathway for THAP when near UV photons are used. The details of the mechanism of thermal ionization will be discussed in a separate work.

Redistribution of Energy in Matrixes. According to the chemical property of the matrix and the excitation conditions, the four components in eq 4 can be reduced for every matrix. The full expression of eq 4 can be applied to CHCA and DHB, for which every term is important in the initial reactions. Because energy is conserved, the distribution of energy among components should be balanced according to the reaction conditions. That is, changing the abundance of one term will change the contributions of all of the others. When all of the

endoergic pathways are considered, the matrix-specific eq 4 near F_{th} becomes

CHCA:

$$E_{laser} = aE_{pi} + bE_{frag} + cE_{flu} + dE_{nonrad}$$

SA:

$$E_{laser} = aE_{pi} + bE_{frag} + dE_{nonrad}$$

DHB:

$$E_{laser} = aE_{pi} + bE_{frag} + cE_{flu} + dE_{nonrad}$$

THAP:

$$E_{laser} = dE_{nonrad} \qquad (\lambda = 337, 355 \text{ nm})$$
$$= aE_{pi} + bE_{frag} + dE_{nonrad} \quad (\lambda = 266 \text{ nm})$$

In the current study, DHB had the lowest I_{IR} mainly because of its highest I_{flu}, as well as its lowest σ_{266} and second lowest σ_{337} and σ_{355}. Its significant fragmentation also suppressed the temperature increase, so the remaining energy may not efficiently have accelerated eq 2 when the 355 nm laser was operated at its F_{th}. An increase of fluorescence intensity of DHB when nonradiative relaxation processes are suppressed by reducing the crystal temperature has also been reported.[70] A similar concept may be applied to explain the moderate I_{IR} of CHCA, which has the highest σ in all λ_{laser} but the second highest I_{flu}. Nevertheless, CHCA and DHB are popular matrixes for MALDI, so a matrix that can produce high temperature during laser excitation does not necessarily provide good ion yield. The situation for SA and THAP is simpler because the value of c is unimportant, and a and b are negligible for THAP when the 355 nm laser is used.

To establish a quantitative interpretation of the ion yield, it is necessary to determine quantitatively the impact of all initial reactions. The important parameters include the chemical properties of matrixes and the excitation conditions. Although no noticeable difference was observed between the initial reactions that were excited by 337 and 355 nm lasers, different results were obtained with the 266 nm laser. Therefore, an observation is only a specific outcome in response to the particular experimental condition. The chemical equilibrium interpretation of THAP when excited by a 355 nm laser[57] presented to be an ideal case because only the thermal ionization is activated.

■ CONCLUSION

The initial endoergic reactions in MALDI compete with each other for the absorbed laser energy and consequently affect ion production. Their branching ratios are assumed to reach dynamic balances that depend on the properties of the matrix and the excitation method. The ionization may occur via multiple pathways; important examples include photoionization and thermal ionization that occur in the excited and ground states, respectively. Photoionization plays an important role when the matrix has a high absorption cross section or an excited-state lifetime that is on the nanosecond range, such as in the case of CHCA and DHB. While significant energy is converted to thermal energy, thermal ionization may also be induced in the ground state with the energy of a single near UV laser photon. An ideal example is THAP that does not show a long excited-state lifetime or significant decomposition when

excited by a near UV laser. SA represents another distinctive category, in which photoionization is still important due to the high absorption cross section, even though it does not exhibit an excited-state lifetime on the nanosecond range. Owing to the specific ionization property of the individual matrix, the selection of matrix is understandably critical to MALDI. In practice, development of a single ionization model that can be applied universally to all experimental conditions is unlikely; an inactive ionization channel under a specific condition may become a dominant channel under other conditions. Further study is necessary to quantitatively elucidate the contribution of every possible ionization channel to the primary ion yield when the excitation condition is changed. On the basis of the findings of the present study, a temperature regulation method to improve the ion yield of fragile molecules is currently under development, which will be discussed in subsequent reports.

■ ASSOCIATED CONTENT

Ⓢ Supporting Information

Mixed crystal absorption spectra and changes of absorbance with concentration of matrixes, comparison of numerical models for analyzing fluorescence of DHB, mass spectra of matrixes recorded at ion appearance thresholds, and IR emission of matrixes with various laser conditions. This material is available free of charge via the Internet at http://pubs.acs.org.

■ AUTHOR INFORMATION

Corresponding Author

*Mailing address: Genomics Research Center, Academia Sinica, 128, Academia Road, Section 2, Nankang District, Taipei 115, Taiwan, R. O. C. Phone: 886-2-27871272. Fax: 886-2-27899931. E-mail: wer@gate.sinica.edu.tw.

Notes

The authors declare no competing financial interest.

■ ACKNOWLEDGMENTS

■ REFERENCES

(1) Tanaka, K.; Waki, H.; Ido, Y.; Akita, S.; Yoshida, Y.; Yoshida, T. *Rapid Commun. Mass Spectrom.* **1988**, *2*, 151−153.

(2) Karas, M.; Hillenkamp, F. *Anal. Chem.* **1988**, *60*, 2299−2301.

(3) Glish, G.; Vachet, R. *Nat. Rev. Drug Discov.* **2003**, *2*, 140−150.

(4) Bakhtiar, R.; Tse, F. L. S. *Mutagenesis* **2000**, *15*, 415−430.

(5) Aebersold, R.; Goodlett, D. R. *Chem. Rev.* **2001**, *101*, 269−295.

(6) Aebersold, R.; Mann, M. *Nature* **2003**, *422*, 198−207.

(7) Harvey, D. *Mass Spectrom. Rev.* **1999**, *18*, 349−450.

(8) Nielen, M. W. F. *Mass Spectrom. Rev.* **1999**, *18*, 309−344.

(9) Hillenkamp, F.; Peter-Katalinic, J. *MALDI MS: A Practical Guide to Instrumentation, Methods and Applications*; Wiley-VCH: Weinheim, Germany, 2007.

(10) Zenobi, R.; Knochenmuss, R. *Mass Spectrom. Rev.* **1998**, *17*, 337−366.

(11) Karas, M.; Gluckmann, M.; Schafer, J. *J. Mass Spectrom.* **2000**, *35*, 1−12.

(12) Kaufmann, R.; Spengler, B.; Lutzenkirchen, F. *Rapid Commun. Mass Spectrom.* **1993**, *7*, 902−910.

(13) Dreisewerd, K. *Chem. Rev.* **2003**, *103*, 395−425.

(14) Knochenmuss, R.; Zenobi, R. *Chem. Rev.* **2003**, *103*, 441−452.

(15) Karas, M.; Kruger, R. *Chem. Rev.* **2003**, *103*, 427−439.

(16) Knochenmuss, R.; Dubois, F.; Dale, M. J.; Zenobi, R. *Rapid Commun. Mass Spectrom.* **1996**, *10*, 871−877.

(17) Knochenmuss, R. *Analyst* **2006**, *131*, 966−986.

(18) Liao, P. C.; Allison, J. *J. Mass Spectrom.* **1995**, *30*, 408−423.

(19) Karbach, V.; Knochenmuss, R. *Rapid Commun. Mass Spectrom.* **1998**, *12*, 968−974.

(20) Knochenmuss, R. *J. Mass Spectrom.* **2002**, *37*, 867−877.

(21) Zhigilei, L. V.; Yingling, Y. G.; Itina, T. E.; Schoolcraft, T. A.; Garrison, B. J. *Int. J. Mass Spectrom.* **2003**, *226*, 85−106.

(22) Gluckmann, M.; Pfenninger, A.; Kruger, R.; Thierolf, M.; Karas, M.; Horneffer, V.; Hillenkamp, F.; Strupat, K. *Int. J. Mass Spectrom.* **2001**, *210*, 121−132.

(23) Chen, X. J.; Carroll, J. A.; Beavis, R. C. *J. Am. Soc. Mass Spectrom.* **1998**, *9*, 885−891.

(24) Ehring, H.; Karas, M.; Hillenkamp, F. *Org. Mass Spectrom.* **1992**, *27*, 472−480.

(25) Ehring, H.; Costa, C.; Demirev, P. A.; Sundqvist, B. U. R. *Rapid Commun. Mass Spectrom.* **1996**, *10*, 821−824.

(26) Dreisewerd, K.; Schurenberg, M.; Karas, M.; Hillenkamp, F. *Int. J. Mass Spectrom. Ion Process.* **1995**, *141*, 127−148.

(27) Setz, P. D.; Knochenmuss, R. *J. Phys. Chem. A* **2005**, *109*, 4030−4037.

(28) Allwood, D. A.; Dyer, P. E.; Dreyfus, R. W. *Rapid Commun. Mass Spectrom.* **1997**, *11*, 499−503.

(29) Horneffer, V.; Dreisewerd, K.; Ludemann, H. C.; Hillenkamp, F.; Lage, M.; Strupat, K. *Int. J. Mass Spectrom.* **1999**, *187*, 859−870.

(30) Yao, J.; Scott, J. R.; Young, M. K.; Wilkins, C. L. *J. Am. Soc. Mass Spectrom.* **1998**, *9*, 805−813.

(31) Tsai, S.-T.; Chen, C.-H.; Lee, Y. T.; Wang, Y.-S. *Mol. Phys.* **2008**, *106*, 239−247.

(32) Chen, Y.; Vertes, A. *J. Phys. Chem. A* **2003**, *107*, 9754−9761.

(33) Vorm, O.; Roepstorff, P.; Mann, M. *Anal. Chem.* **1994**, *66*, 3281−3287.

(34) Dreisewerd, K.; Berkenkamp, S.; Leisner, A.; Rohlfing, A.; Menzel, C. *Int. J. Mass Spectrom.* **2003**, *226*, 189−209.

(35) Ludemann, H. C.; Redmond, R. W.; Hillenkamp, F. *Rapid Commun. Mass Spectrom.* **2002**, *16*, 1287−1294.

(36) Bourcier, S.; Bouchonnet, S.; Hoppilliard, Y. *Int. J. Mass Spectrom.* **2001**, *210/211*, 59−69.

(37) Frankevich, V.; Knochenmuss, R.; Zenobi, R. *Int. J. Mass Spectrom.* **2002**, *220*, 11−19.

(38) Knochenmuss, R. *Anal. Chem.* **2004**, *76*, 3179−3184.

(39) Dashtiev, M.; Wafler, E.; Rohling, U.; Gorshkov, M.; Hillenkamp, F.; Zenobi, R. *Int. J. Mass Spectrom.* **2007**, *268*, 122−130.

(40) Knochenmuss, R. *Int. J. Mass Spectrom.* **2008**, *273*, 84−86.

(41) Hillenkamp, F.; Wafler, E.; Jecklin, M. C.; Zenobi, R. *Int. J. Mass Spectrom.* **2009**, *285*, 114−119.

(42) Frankevich, V. E.; Zhang, J.; Friess, S. D.; Dashtiev, M.; Zenobi, R. *Anal. Chem.* **2003**, *75*, 6063−6067.

(43) Tsai, S.-T.; Chen, C. W.; Huang, L. C. L.; Huang, M.-C.; Chen, C.-H.; Wang, Y.-S. *Anal. Chem.* **2006**, *78*, 7729−7734.

(44) Liu, B.-H.; Lee, Y. T.; Wang, Y.-S. *J. Am. Soc. Mass Spectrom.* **2009**, *20*, 1078−1086.

(45) Liu, B. H.; Charkin, O. P.; Klemenko, N.; Chen, C. W.; Wang, Y. S. *J. Phys. Chem. B* **2010**, *114*, 10853−10859.

(46) Koubenakis, A.; Frankevich, V.; Zhang, J.; Zenobi, R. *J. Phys. Chem. A* **2004**, *108*, 2405−2410.

(47) Schulz, E.; Karas, M.; Rosu, F.; Gabelica, V. *J. Am. Soc. Mass Spectrom.* **2006**, *17*, 1005−1013.

(48) Luo, G. H.; Marginean, I.; Vertes, A. *Anal. Chem.* **2002**, *74*, 6185−6190.

(49) Bae, Y. J.; Moon, J. H.; Kim, M. S. *J. Am. Soc. Mass Spectrom.* **2011**, *22*, 1070−1078.

(50) Gabelica, V.; Schulz, E.; Karas, M. *J. Mass Spectrom.* **2004**, *39*, 579−593.

(51) Mowry, C. D.; Johnston, M. V. *J. Phys. Chem.* **1994**, *98*, 1904−1909.

(52) Zhigilei, L. V.; Leveugle, E.; Garrison, B. J.; Yingling, Y. G.; Zeifman, M. I. *Chem. Rev.* **2003**, *103*, 321−347.

(53) Zhigilei, L. V.; Garrison, B. J. *J. Appl. Phys.* **2000**, *88*, 1281−1298.

(54) Allwood, D. A.; Dyer, P. E. *Chem. Phys.* **2000**, *261*, 457−467.

(55) Ehring, H.; Sundqvist, B. U. R. *Appl. Surf. Sci.* **1996**, *96−8*, 577−580.

(56) Cosa, G.; Focsaneanu, K. S.; McLean, J. R. N.; McNamee, J. P.; Scaiano, J. C. *Photochem. Photobiol.* **2001**, *73*, 585−599.

(57) Lai, Y. H.; Wang, C. C.; Lin, S. H.; Lee, Y. T.; Wang, Y. S. *J. Phys. Chem. B* **2010**, *114*, 13847−13852.

(58) Barone, V.; Cossi, M.; Tomasi, J. *J. Chem. Phys.* **1997**, *107*, 3210−3221.

(59) Tomasi, J.; Mennucci, B.; Cammi, R. *Chem. Rev.* **2005**, *105*, 2999−3093.

(60) Allwood, D. A.; Dreyfus, R. W.; Perera, I. K.; Dyer, P. E. *Rapid Commun. Mass Spectrom.* **1996**, *10*, 1575−1578.

(61) Schlag, E. W. *Zeke Spectroscopy*; Cambridge University Press: Cambridge, U.K.; New York, 1998.

(62) Lin, S. H. *Multiphoton Spectroscopy of Molecules*; Academic Press: Orlando, FL, 1984.

(63) Hoyer, T.; Tuszynski, W.; Lienau, C. *Chem. Phys. Lett.* **2007**, *443*, 107−112.

(64) Wallace, W. E.; Arnould, M. A.; Knochenmuss, R. *Int. J. Mass Spectrom.* **2005**, *242*, 13−22.

(65) Pshenichnyuk, S. A.; Asfandiarov, N. L. *Eur. J. Mass Spectrom.* **2004**, *10*, 477−486.

(66) Jaskolla, T. W.; Karas, M. *J. Am. Soc. Mass Spectrom.* **2008**, *19*, 1054−1061.

(67) Kosaka, T.; Kinoshita, T.; Takayama, M. *Rapid Commun. Mass Spectrom.* **1996**, *10*, 405−408.

(68) Land, C. M.; Kinsel, G. R. *J. Am. Soc. Mass Spectrom.* **1998**, *9*, 1060−1067.

(69) Bagchi, A.; Dyakov, Y. A.; Ni, C. K. *J. Chem. Phys.* **2010**, *133*.

(70) Ehring, H.; Sundqvist, B. U. R. *J. Mass Spectrom.* **1995**, *30*, 1303−1310.

(71) Cramer, R.; Hillenkamp, F.; Haglund, R. F. *J. Am. Soc. Mass Spectrom.* **1996**, *7*, 1187−1193.

(72) Niu, S. F.; Zhang, W. Z.; Chait, B. T. *J. Am. Soc. Mass Spectrom.* **1998**, *9*, 1−7.

(73) Little, M. W.; Kim, J. K.; Murray, K. K. *J. Mass Spectrom.* **2003**, *38*, 772−777.

(74) Lide, D. R. *CRC Handbook of Chemistry and Physics: A Ready-Reference Book of Chemical and Physical Data*, 87th ed.; CRC Press: Boca Raton, FL, 2006.